Chemical Engineering Science 300 (2024) 120551

Contents lists available at ScienceDirect

Chemical Engineering Science

journal homepage: www.elsevier.com/locate/ces

Modeling reactive film flows down a heated fiber

Souradip Chattopadhyay, Hangjie Ji *

Department of Mathematics, North Carolina State University, Raleigh, NC 27695, USA

ARTICLE INFO

Keywords:
Thin films
Chemical reaction
Vertical fiber
Van der Waals attractions
Marangoni effect
Nonlinear stability

ABSTRACT

We study the dynamics of an ultra-thin reactive liquid film flowing down a heated vertical fiber under the influence of gravity. A key focus is on the impact of the van der Waals attraction, which is proportional to h^{-3}, where h denotes the film thickness. Linear stability analysis of the film flow reveals that the van der Waals attractions and the Marangoni effect enhance the instability. Furthermore, instability is reduced by exothermic chemical reactions, while it is strengthened in the case of endothermic chemical reactions. Moreover, the weakly nonlinear stability of the film flow is studied. The results indicate the possibility of both subcritical and supercritical stability in the system. Lastly, direct numerical simulations of the evolution equation are conducted for various flow parameters. These results enhance our understanding of the intricate interplay of chemical reactions, thermal effects, and intermolecular forces influencing the liquid film dynamics in complex systems.

1. Introduction

The interfacial dynamics of thin liquid films flowing down vertical fibers have attracted considerable attention due to their complexity (Craster and Matar, 2009; Oron et al., 1997) and wide range of applications (Ji et al., 2021; Quéré, 1999; Zeng et al., 2017). Notable phenomena include the formation of droplets and the emergence of traveling wave patterns (Kalliadasis et al., 2012; Quéré, 1990). Exploring the flow of thin films along heated vertical fibers is particularly intriguing as it has diverse practical applications, such as the cooling of optical fibers (Sweetland and Lienhard, 2000) and the condensation of vapor on heat pipes (Kundan et al., 2017). The flow of a thin film along a heated cylindrical surface introduces non-uniformity in its profile, which in turn creates temperature gradients at the liquid-air interface. Previous studies (Dávalos-Orozco and You, 2000; Ding and Wong, 2017; Mukhopadhyay et al., 2020) have shown that when the film is situated on the exterior or interior of a heated cylinder, these interfacial thermal gradients generate unbalanced thermocapillary stress, leading to a destabilizing influence on the film. Several modeling approaches have been developed to examine the dynamics of exterior coating flows on fibers with or without thermal effects. These approaches include thin film models (Frenkel, 1992; Kalliadasis and Chang, 1994), thick film models (Kliakhandler et al., 2001), asymptotic models (Craster and Matar, 2006), weighted residual models (Ruyer-Quil et al., 2008), and integral boundary layer models (Shkadov et al., 2008). More recently, Kim et al. (2024), and Biswal et al. (2024) have developed positivity-preserving numerical schemes and optimal boundary control strategies within the context of fiber coating models.

Thin liquid films flowing down vertical fibers under the influence of gravity display interesting dynamics, such as the formation of viscous beads and the breakup of the film. In the absence of additional effects like the Marangoni effect, the flow of a falling film over cylindrical substrates becomes hydrodynamically unstable primarily due to the well-known Rayleigh-Plateau (RP) instability (Quéré, 1999). In such flow scenarios, thin films can fragment into droplets on cylindrical surfaces, while cylindrical threads and jets manifest regular droplet-like wave patterns due to the RP mechanism (Rayleigh, 1892). Lister et al. (2006) reported the emergence of collars and lobes with the RP mechanism. Moreover, the literature suggests that thermocapillarity may enhance the RP instability, potentially leading to finite-time film rupture (Liu and Liu, 2014).

The rupture of thin, viscous liquid films on flat surfaces or vertical fibers poses an intriguing challenge. The emergence of holes or dry patches in a uniform fluid layer leads to localized singularities in finite time, subsequently altering the topology and structure of fluid flow within the layer (Herminghaus et al., 1998; Xie et al., 1998). These considerations are particularly significant in the coating industry, including optical coatings and insulating layers in micro-circuitry, where non-uniformities are undesirable (Oron et al., 1997). Previous studies by Williams and Davis (1982), Reisfeld and Bankoff (1992), Bertozzi and Pugh (1998), Witelski and Bernoff (2000), Hatziavramidis (1992) and Matar (2002) have explored the thin film instabilities induced by

* Corresponding author.
E-mail addresses: schatto5@ncsu.edu (S. Chattopadhyay), hangjie_ji@ncsu.edu (H. Ji).

https://doi.org/10.1016/j.ces.2024.120551
Received 21 March 2024; Received in revised form 3 July 2024; Accepted 22 July 2024
Available online 30 July 2024

intermolecular forces. These studies typically involve thin films with thicknesses ranging from 100 to 1000 angstroms, subjected to long-range van der Waals interactions that can lead to finite-time rupture (Sheludko, 1967). In addition to van der Waals forces, previous investigations have considered factors such as surface tension, evaporation, condensation, surfactants, slip, and various other scenarios. However, it is important to note that the studies on the vertical fibers or cylinders (Craster and Matar, 2006; Frenkel, 1992; Kalliadasis and Chang, 1994; Kliakhandler et al., 2001; Ruyer-Quil et al., 2008; Shkadov et al., 2008) did not incorporate the effects of van der Waals attractions. Ding et al. (2019) investigated the behavior of ultra-thin liquid films on a heated vertical fiber. They considered the influence of van der Waals attraction to predict the film breakup. Their results revealed that an isothermal film consistently undergoes breakup in the absolutely unstable regime in the presence of van der Waals attractions. Importantly, they concluded that the Marangoni effect significantly accelerates the breakup process.

To describe liquid wetting/dewetting on solid surfaces, intermolecular forces such as van der Waals interactions are included in the dynamic pressure using a disjoining pressure, denoted as $\Pi(h)$, in lubrication equations. Ruckenstein and Jain (1974), Reisfeld and Bankoff (1992) and Burelbach et al. (1988) characterized van der Waals forces as $\Pi(h) = Ah^{-3}$, where A is the Hamaker constant. These forces destabilize when $A > 0$, while $A < 0$ leads to stabilization. Ji et al. (2019) investigated a liquid film flowing along the outer surface of a vertical fiber with a film stabilization term that takes the functional form of the disjoining pressure $\Pi(h) = Ah^{-3}$ with $A < 0$ as a stabilization parameter. For a dewetting liquid, the purely destabilizing intermolecular forces modeled by $\Pi(h) = Ah^{-3}$ with $A > 0$ can result in finite-time rupture of the film thickness.

Despite the advances in the study of thin film flows, theoretical developments on the influence of chemical reactions on thin film flows are still lacking. In 1984, Dagan and Pismen (1984) investigated the connection between chemical reactions and thin film hydrodynamics. The study by Gallez et al. (1996) explored the dynamics of a thin liquid film undergoing a surface chemical reaction. They focused on the interaction between insoluble surfactants on the liquid-air interface and substrate binding sites. The researchers demonstrated that the coupling between the thin film and the chemical reaction substantially influenced its dynamics, resulting in oscillatory behavior and rupture. Braun et al. (1995) investigated how temperature-dependent surface tension affects the spreading of a drop on a solid plate in the presence of an isothermal chemical reaction. Subsequently, Trevelyan et al. (2002) and Trevelyan and Kalliadasis (2004a,b) studied the progression of a vertically falling film undergoing a first-order exothermic chemical reaction. These studies provided evidence that an exothermic reaction exerted a stabilizing effect on the free surface. These studies further revealed that the presence of chemical reactions can significantly impact the evolution of the interface, leading to dispersive solitary waves. Matar and Spelt (2005) investigated the dynamics of thin liquid films under exothermic chemical reactions, which induce changes in film density and viscosity. Pereira et al. (2007) examined the interplay between a reaction-diffusion process and the hydrodynamics of a horizontal thin liquid film. They found that this interplay had a significant influence on the flow dynamics. The free surface was linearly stable when the Marangoni effect was not present. However, the coupling between the free surface and the linearly unstable reaction-diffusion system, facilitated by the Marangoni effect, led to its destabilization. In subsequent studies, Trevelyan et al. (2012), Chao et al. (2020), Li and Chao (2020), and Chattopadhyay (2023) observed notable effects while investigating the behavior of a thin film flowing down an inclined plane and a cylindrical surface, respectively. These investigations were conducted in the presence of a first-order chemical reaction and under the influence of gravity.

It has been established that the presence of van der Waals attractions and the Marangoni effect results in an increased RP instability (Ding et al., 2019). However, the impact of chemical reactions on the instability induced by both thermal effects and van der Waals attraction remains unexplored. The present study aims to investigate whether this instability can be mitigated by chemical reactions. Understanding the dynamics of reactive film flows is crucial for coating flow applications in industrial settings (Kundan et al., 2017; Quéré, 1990; Sweetland and Lienhard, 2000; Zeng et al., 2017), especially those involving first-order reactions, such as catalytic or acid-base reactions. For example, combustion chambers, fuels, and engine oils create wall films, resulting in deposits on ports, cylinder walls, and pistons (Zhao et al., 1999). These deposits, formed through chemical reactions (Dagaut et al., 2002; Norinaga and Deutschmann, 2007), diminish engine efficiency and increase pollutant emissions. Trevelyan et al. (2012) briefly discussed the practical scenarios with chemical reactions of this nature. To our knowledge, there have been no studies on the delay or mitigation of the rupture phenomena of thin liquid films on heated fibers with van der Waals attractions. Our model offers new insights into the dynamics and parametric study of chemical reaction aspects in coating processes within chemical engineering and could serve as a resource for further exploration in this area. Furthermore, the findings of this study could provide insights for enhancing the quality of coating films on cylindrical surfaces and suggest a new direction for utilizing chemical reactions to achieve smooth textures in various products like paper and microchips.

The subsequent sections of the paper are structured as follows. In Section 2, a thin film model is formulated that incorporates exothermic or endothermic chemical reactions and includes van der Waals attractions. A single nonlinear equation is constructed that describes the evolution of the thin liquid film interface. Further, a linear and weakly nonlinear stability analysis is performed in Section 3. Furthermore, in Section 4, a direct numerical simulation of the nonlinear evolution equation is carried out. The key findings are discussed in Section 5.

2. Mathematical model

The problem under consideration involves a vertical cylindrical fiber with uniform surface temperature T_s, over which an ultra-thin Newtonian liquid film flows, as shown in Fig. 1. The study assumes axisymmetry and uses cylindrical coordinates (r, z). The thickness of the liquid film at any time is denoted by $h(z, t)$, while the fiber has a radius R. The surrounding air is assumed to be inviscid, and thus, its dynamics are neglected. The species $\mathcal{Z}_1$ is present in the ambient gas phase and absorbed at the interface into the liquid film, which is always saturated with $\mathcal{Z}_1$ due to its infinite availability in the gas phase. The reaction undergoes a simple first-order process, represented by $\mathcal{Z}_1 \rightarrow \mathcal{Z}_2 \pm$ heat (Li and Chao, 2020; Trevelyan and Kalliadasis, 2004a; Trevelyan et al., 2002). Both $\mathcal{Z}_1$ and $\mathcal{Z}_2$ are considered passive species, i.e., their concentration profiles do not affect the flow field. The system involves several variables, namely $\mathcal{U} = (u_1, u_2)$ representing the radial and axial velocity components, pressure p, temperature T, and concentration $\varkappa$ of species $\mathcal{Z}_1$. The system also involves density ρ, dynamic viscosity μ, thermal diffusivity κ, and molecular diffusivity d_{mol} of species $\mathcal{Z}_1$. The reaction rate coefficient (b) is assumed to be temperature-independent (Petrucci, 2017). Following Chao et al. (2020); Li and Chao (2020), this study considers only the thermocapillary Marangoni effect and neglects the solutocapillary Marangoni effect, which can arise from the solute concentration gradient (Dagan and Pismen, 1984).

We provide the dimensional system of equations in Appendix A. Let us simplify the analysis by introducing the following dimensionless variables based on the film geometry (Chao et al., 2020)

$$(r, z) = \mathcal{H}\left(r^*, z^*\right), t = (\mathcal{H}/\mathcal{V})\, t^*, \left(u_1, u_2\right) = \mathcal{V}\left(u_1^*, u_2^*\right),$$
$$p = p_\infty + \rho g \mathcal{H} p^*, T = T_\infty + T^* \Delta T, \varkappa = C\varkappa^*, \tag{1}$$

where the variable with an asterisk denotes a dimensionless quantity, the acceleration due to gravity is denoted by g, $\mathcal{H}$ is the mean film thickness, $\mathcal{V} = \rho g \mathcal{H}^2/\mu$ is the characteristic velocity, $\Delta T = T_s - T_\infty$, C is

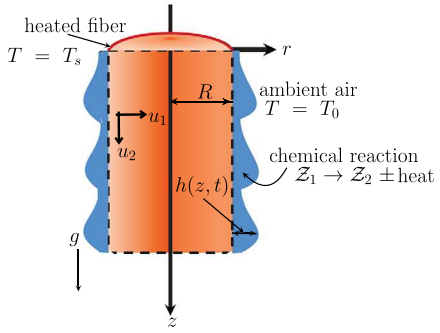

Fig. 1. Model geometry.

the initial concentration of species $\mathcal{Z}_1$ in the film, and p_∞ is the ambient pressure.

Inserting (1) into the dimensional system of equations, the motion of the liquid can be described by the following dimensionless equations after omitting the asterisks:

$$\nabla \cdot \mathcal{U} = 0, \tag{2}$$

$$Re\frac{D\mathcal{U}}{Dt} = 1 - \nabla p + \nabla^2 \mathcal{U}, \tag{3}$$

$$RePr\frac{DT}{Dt} = \nabla^2 T + \Phi \mathcal{D}_a \varkappa, \tag{4}$$

$$ReS\frac{D\varkappa}{Dt} = \nabla^2 \varkappa - \mathcal{D}_a \varkappa, \tag{5}$$

$$\mathcal{U} = \mathbf{0},\ T = 1,\ \varkappa_r = 0 \quad \text{at } r = \alpha, \tag{6}$$

$$\frac{A_{\mathrm{H}}}{h^3}\mathbf{n} + \left[-p\mathbb{I} + \nabla\mathcal{U} + (\nabla\mathcal{U})^{\mathrm{T}}\right]\cdot\mathbf{n} = -Mn\nabla_s T^i - \frac{1-\Lambda T^i}{Ca}(\nabla\cdot\mathbf{n})\mathbf{n}$$
$$\text{at } r = \alpha + h(z,t), \tag{7}$$

$$u_1 = h_t + u_2 h_z \quad \text{at } r = \alpha + h(z,t), \tag{8}$$

$$\nabla T \cdot \mathbf{n} + BiT = 0 \quad \text{at } r = \alpha + h(z,t), \tag{9}$$

$$\varkappa = 1 \quad \text{at } r = \alpha + h(z,t), \tag{10}$$

where $\mathbf{n}$ represent the unit normal vector, $\mathbb{I}$ denote the identity tensor, ∇ be the gradient operator, $D/Dt = \partial_t + \mathcal{U}\cdot\nabla$ represent the material derivative, and $\nabla_s = \nabla - \mathbf{n}(\mathbf{n}\cdot\nabla)$ denote the surface gradient operator. The system is characterized by various dimensionless parameters, including $\alpha = R/\mathcal{H}$, Reynolds number $Re = \rho\mathcal{V}\mathcal{H}/\mu$, Prandtl number $Pr = \mu/(\rho\kappa)$, Damköhler number $\mathcal{D}_a = b\mathcal{H}^2/d_{\mathrm{mol}}$, dimensionless heat of reaction $\Phi = YCd_{\mathrm{mol}}/(\kappa\Delta T)$, Schmidt number $S = \mu/\left(\rho d_{\mathrm{mol}}\right)$, Marangoni number $Mn = \gamma\Delta T/(\mu\mathcal{V})$, capillary number $Ca = \mu\mathcal{V}/\sigma_0$, $\Lambda = \gamma\Delta T/\sigma_0$, and Biot number $Bi = \mathcal{H}k_g/\lambda$. We introduce a composite Hamaker number $A_{\mathrm{H}} = \mathcal{G}/Re$ to represent the strength of van der Waals attractions, where $\mathcal{G} = A'/\left(6\pi\mathcal{H}\rho\nu^2\right)$ is the dimensionless Hamaker constant and A' is the dimensional Hamaker constant. When $\mathcal{D}_a = 0$, it indicates the absence of chemical reactions (Trevelyan et al., 2002). Similarly, when $\Phi = 0$, the chemical reaction is assumed to be isothermal. The heat generated or absorbed by the chemical reaction is denoted by Y, which is assumed to be independent of temperature. For exothermic reactions, Y is positive, whereas for endothermic reactions, Y is negative (Chao et al., 2020). The system of equations (2)-(10) matches Ding et al. (2019) without chemical reactions and Chao et al. (2020) without van der Waals attraction.

The system of equations is derived under the assumption that the surface tension σ varies linearly with temperature and can be expressed as (Chattopadhyay (2021a, 2024); Chattopadhyay and Ji (2023)): $\sigma(T) = \sigma_0 - \gamma\left(T^i - T_0\right)$. The coefficient $\gamma > 0$ represents the thermal surface tension coefficient, which characterizes the rate of change of surface tension to temperature evaluated at the reference temperature T_0. This assumption is valid when the temperature difference between T^i and T_0 is small, where T^i is the temperature at the interface of the liquid film. Ding et al. (2018) estimated Λ of castor oil to be $O\left(10^{-2}\right)$ using a temperature difference of approximately 10 K. Since Λ is negligible, we will ignore it for further discussion.

To construct the equation of the liquid-air interface, we assume $\mathcal{H} \ll R$ and introduce a small parameter $\delta = \mathcal{H}/R \ll 1$. Consequently, we introduce the following transformations (Chao et al., 2018):

$$t \rightarrow \delta^2 t, \quad r = \alpha + \delta y, \quad h \rightarrow \delta H. \tag{11}$$

The variables u_1, u_2, p, T and $\varkappa$ are expanded as follows (Chao et al., 2020; Li and Chao, 2020)

$$u_1 = \delta^3\left(u_1^{(0)} + \delta u_1^{(1)} + \cdots\right),\ u_2 = \delta^2\left(u_2^{(0)} + \delta u_2^{(1)} + \cdots\right),$$
$$(p, T, \varkappa) = \left(p^{(0)}, T^{(0)}, \varkappa^{(0)}\right) + \delta\left(p^{(1)}, T^{(1)}, \varkappa^{(1)}\right) + \cdots. \tag{12}$$

Substituting (11)-(12) into the governing equations (2)-(5) and boundary conditions (6), (7), (9), (10), and taking the limit $\delta \rightarrow 0$, the leading-order terms are given by the following equations

$$u_{1,y}^{(0)} + u_{2,z}^{(0)} = 0, \quad p_y^{(0)} = 0, \quad p_z^{(0)} = 1 + u_{2,yy}^{(0)}, \quad T_{yy}^{(0)} + X\varkappa = 0, \quad \varkappa_{yy}^{(0)} = 0, \tag{13}$$

$$u_1^{(0)} = 0, \quad u_2^{(0)} = 0, \quad T^{(0)} = 1, \quad \varkappa_y^{(0)} = 0 \quad \text{at } y = 0, \tag{14}$$

$$u_{2,y}^{(0)} = -MnT_z^{(0)}, \quad p^{(0)} = \frac{A_{\mathrm{H}}}{H^3} + \frac{1}{Ca}\left(\frac{1}{\delta\alpha} - \frac{H}{\alpha^2} - H_{zz}\right),$$
$$T_y^{(0)} = -BiT^{(0)}, \quad \varkappa^{(0)} = 1 \quad \text{at } y = H. \tag{15}$$

While deriving the equations (13)-(15), we obtained the dimensionless flow parameters Φ, A_{H}, Mn, Ca, Bi, and $\mathcal{D}_a$ as $\delta^2\Phi$, $\delta^{-3}A_{\mathrm{H}}$, $\delta^{-1}Mn$, $\delta^{-1}Ca$, δBi, and $\delta^2\mathcal{D}_a$. The term $\delta^2\mathcal{D}_a$ was neglected due to the assumption of a slow chemical reaction $\left(\mathcal{D}_a \ll 1\right)$ (Chao et al., 2020; Chattopadhyay, 2023). To retain the terms associated with van der Waals attraction (represented by the dimensionless composite Hamaker number A_{H}), thermal effect (represented by Mn), and surface tension (represented by Ca), we rescaled $\delta^{-3}A_{\mathrm{H}}$, $\delta^{-1}Mn$, and $\delta^{-1}Ca$ as $\delta^{-3}A_{\mathrm{H}} \rightarrow \widetilde{A}$, $\delta^{-1}Mn \rightarrow \widetilde{Ma}$, and $\delta^{-1}Ca \rightarrow \widetilde{Ca}$ (Chao et al., 2020; Ding et al., 2019). Additionally, to maintain the effect of the Biot number Bi, we rescaled δBi as $\delta Bi \rightarrow \widetilde{Bi}$. We assumed that these rescaled dimensionless numbers $\widetilde{A}$, $\widetilde{Ma}$, $\widetilde{Ca}$, and $\widetilde{Bi}$ are of order unity. To account the chemical reaction, we have rescaled $\delta^2\Phi$ as $\delta^2\Phi \rightarrow \widetilde{\Phi}$ and introduced a parameter $X = \widetilde{\Phi}\mathcal{D}_a$ into the mass transport equation of (13) (Chao et al., 2020; Li and Chao, 2020). It is important to note that the new parameter X depends on the dimensionless heat of reaction Φ, which is proportional to the parameter Y. This Y parameter signifies the heat generation or absorption by the chemical reaction and is independent of temperature. Therefore, X is essentially proportional to Y. Considering exothermic reactions where Y is positive and endothermic reactions where Y is negative, a positive value of X signifies an exothermic reaction, while a negative value indicates an endothermic reaction.

However, for notational simplicity, we drop the tilde sign from the rescaled flow parameters $\widetilde{A}$, $\widetilde{Ma}$, $\widetilde{Ca}$, and $\widetilde{Bi}$ in our upcoming discussion. The leading order solutions for (13)-(15) are given by

$$T^{(0)} = 1 - \frac{Biy}{1+BiH} - \frac{X}{2}\left(y - \frac{H(2+BiH)}{(1+BiH)}\right)y, \tag{16}$$

$$u_2^{(0)} = \left(p_z^{(0)} - 1\right)\left(\frac{y^2}{2} - Hy\right) - \frac{Ma}{(1+BiH)^2}(XH - Bi)H_z y. \tag{17}$$

The kinematic condition (8) can be expressed as mass conservation at leading order, which yields $H_t + \partial_z\int_0^H u_2^{(0)}dy = 0$. Substituting (17) into the mass conservation equation, the evolution equation for the free surface can be obtained as follows

$$H_t + \underbrace{H^2 H_z}_{\text{term (i)}} + \Bigg[\underbrace{\frac{H^3}{3Ca}\left(\frac{H_z}{\alpha^2} + H_{zzz}\right)}_{\text{term (ii)}} + \underbrace{\frac{AH_z}{H}}_{\text{term (iii)}} - \underbrace{\frac{Ma(XH-Bi)}{2(1+BiH)^2}H^2 H_z}_{\text{term (iv)}}\Bigg]_z = 0. \tag{18}$$

Equation (18) describes the evolution of the liquid-air interface of a Newtonian film along a vertical fiber, taking into account the effects of chemical reactions (parameter X) and van der Waals attractions (parameter A). Unlike the previous work by Chao et al. (2020), which focused solely on the effects of chemical reactions in similar dynamics, this new model incorporates additional physics by including van der Waals attractions. Furthermore, our model equation (18) is comparable to the one in the study by Li and Chao (2020) on chemical reactions on similar dynamics for fluids with surface tension that depends quadratically on temperature (self-rewetting fluid). Specifically, (18) agrees with the model studied in Li and Chao (2020) in the absence of van der Waals attractions and when the surface tension is approximated as a linearly decreasing function of temperature. Our model also aligns with Ding et al. (2019) when chemical reactions are absent ($X = 0$). Here, we physically interpret the various terms in the evolution equation. Firstly, the term (i) arises from the mean flow. Secondly, term (ii) is linked to surface tension, encompassing both azimuthal and axial curvature components, whereas term (iii) emerges due to van der Waals attraction. Term (iv) comprises two components, both connected to the Marangoni number Ma. It is important to note that the Marangoni term appears here due to both chemical reactions and uniform heating. The component MaX arises from the chemical reaction, while the component $MaBi$ stems from the uniform heating of the fiber.

We simplify our analysis by not considering the effects of fiber radius α and capillary number Ca. Consequently assuming $\alpha = Ca = 1$ (Chao et al., 2020; Ding et al., 2019), the evolution equation (18) reduces to

$$H_t + H^2 H_z + \left[\left(\frac{H^3}{3} + \frac{A}{H} - \frac{Ma(XH - Bi)H^2}{2(1 + BiH)^2}\right) H_z + \frac{H^3}{3} H_{zzz}\right]_z = 0. \tag{19}$$

Equation (19) governs the liquid-air interface dynamics, influenced by van der Waals attraction and the Marangoni effect from uniform heating and chemical reactions.

Before discussing model results, we briefly examine parameter values pertinent to experiments outlined in the literature. It is crucial to note that, in the context of this study, a negligible Reynolds number is assumed, denoted as $Re \ll 1$ for the model derivation. Consequently, the applicability of this model is confined to scenarios where the RP instability is anticipated to predominate over the Kapitza instability. For flows with higher Reynolds numbers, one may consider retaining inertial terms in the derivation or adopting an integral boundary layer modeling approach. The latter has successfully aligned with experiments conducted at moderate to high liquid Reynolds numbers.

First, we estimate the range of the dimensionless number A, which characterizes the impact of van der Waals attraction. Based on our model formulation, A is linked to the dimensionless composite Hamaker number A_{H} as $A = \delta^{-3} A_{\mathrm{H}}$, where $A_{\mathrm{H}} = \mathcal{G}/Re$ and $\mathcal{G} = A'/\left(6\pi \mathcal{H} \rho \nu^2\right)$ is the dimensionless Hamaker constant. Burelbach et al. (1988) determined that A' is of the order $O\left(10^{-20}\right)$ N m. Let us consider the water for example: density $\rho = 10^3$ kg m^{-3} and viscosity $\mu = 10^{-3}$ N m^{-2}s. Assuming $\mathcal{H} = 10^{-5}$ m and $A' \sim O\left(10^{-20}\right)$ N m, we obtain the velocity scale $\mathcal{V} = \rho g \mathcal{H}^2/\mu = 9.81 \times 10^{-4}$ m s^{-1}, the dimensionless Hamaker number $\mathcal{G} = 5.3 \times 10^{-8}$ and the Reynolds number $Re = 9.81 \times 10^{-3}$. Therefore, the dimensionless composite Hamaker number A_{H} we obtain as $A_{\mathrm{H}} = 5 \times 10^{-6}$. According to our model assumption, δ is small, and we consider δ to be approximately of order $O\left(10^{-1}\right)$. Consequently, A is approximately $O\left(10^{-3}\right)$. However, for the theoretical discussion of the present model, we will consider slightly stronger intermolecular forces with A in the range of $O\left(10^{-2}\right) - O\left(10^{-1}\right)$.

Next, let us estimate the range of the Marangoni number Ma. According to our model formulation, Ma is related to the Marangoni number Mn as $Ma = \delta^{-1} Mn$. Considering water as example with mean film thickness $\mathcal{H} = 5 \times 10^{-4}$ m and $\gamma = 5 \times 10^{-5}$ N m^{-1}K^{-1}, we obtain the Marangoni number $Mn = \gamma \Delta T/(\mu \mathcal{V})$ as $Mn \approx 2 \times 10^{-2} \Delta T$. Assuming ΔT is in the range of 10 K to 20 K, the range of Mn is approximately 0.2 to 0.4. Considering $\delta \sim O\left(10^{-1}\right)$, we determine the range for Ma as 2 to 4. Therefore, for this study, we will adopt the range of Ma as 0 to 4.

3. Stability analysis

We consider the stability analysis of the base state $\bar{h} = 1$ and consequently impose a small disturbance to the film as

$$H(z,t) = 1 + \vartheta(z,t) \tag{20}$$

where $\vartheta(z,t) \ll 1$ represents the small perturbation to the base state at time t.

Substituting (20) into (19) and keeping terms up to $O\left(\vartheta^3\right)$ yields

$$\begin{aligned}&\vartheta_t + \mathcal{M}\vartheta_z + \mathcal{F}\vartheta_{zz} + \mathcal{T}\vartheta_{zzzz} + \mathcal{M}'\vartheta\vartheta_z + \mathcal{F}'\left(\vartheta\vartheta_{zz} + \vartheta_z^2\right)\\ &+\mathcal{T}'\left(\vartheta_{zzzz} + \vartheta_z\vartheta_{zzz}\right) + \frac{1}{2}\mathcal{M}''\vartheta^2\vartheta_z\\ &+\mathcal{F}''\left(\frac{1}{2}\vartheta^2\vartheta_{zz} + \vartheta\vartheta_z^2\right) + \mathcal{T}''\left(\frac{1}{2}\vartheta^2\vartheta_{zzzz} + \vartheta_z\vartheta_{zzz}\right) = 0,\end{aligned} \tag{21}$$

where $\mathcal{M}(H) = H^2$, $\mathcal{F}(H) = \left(H^3/3\right) + AH^{-1} - \frac{Ma}{2(1+BiH)^2}(XH - Bi)H^2$ and $\mathcal{T}(H) = H^3/3$. The values of $\mathcal{M}$, $\mathcal{F}$, $\mathcal{T}$, and their corresponding derivatives are determined at $H = 1$.

For the linear stability analysis, nonlinear terms of (21) are ignored. Normal mode solution assumes $\vartheta \propto \exp[i(kz - \omega t)] + cc$, where k is the wavenumber, $i = \sqrt{-1}$, and $\omega = \omega_r + i\omega_i$ is the complex frequency with ω_r and ω_i being the real and imaginary parts of ω, respectively. The cc denotes the complex conjugate of the preceding term. The dispersion relation is obtained by inserting ϑ in the linearized part of (21) which yields $\omega_r = k$ and

$$\omega_i = \left[\frac{1}{3} + A - \frac{Ma(X - Bi)}{2(1 + Bi)^2}\right] k^2 - \frac{k^4}{3}. \tag{22}$$

Equation (22) reveals that the linear growth rate ω_i is influenced by the van der Waals attractions (through the parameter A), thermocapillary force (via Ma), and the chemical reactions (via X). This implies that these factors significantly impact the film's stability, as even small variations in these parameters can cause changes in the growth rate of disturbances. On the other hand, the linear phase velocity, given by $c_L = \omega_r/k = 1$, is independent of these key parameters. A similar observation was also reported by Chao et al. (2020). Overall, (22) highlights the interplay between various physical mechanisms in determining the stability properties of thin films and underscores the importance of understanding these mechanisms to predict and control the behavior of thin film systems. The sign of ω_i determines the stability of the flow, where a positive value indicates instability and a negative value indicates stability.

In Fig. 2, the impact of the thermocapillary force and van der Waals attractions on the linear growth rate ω_i without chemical reactions ($X = 0$) is illustrated. Fig. 2a shows the enhancement of instability due to substrate heating for three typical Ma values, namely $Ma = 1, 2$ and 4, in the absence of the Hamaker number A. Fig. 2b demonstrates the intensification of instability with increasing van der Waals attractions for three typical Hamaker numbers, namely $A = 0, 0.1$ and 0.2, without the heating effect ($Ma = 0$). Based on these results, it can be concluded that both van der Waals attractions and thermocapillary force enhance the RP instability, which aligns with the findings reported by Ding et al. (2019).

Fig. 3 illustrates the influence of chemical reactions (X) on the linear growth rate under substrate heating and van der Waals attractions. For characterization, we set the Marangoni number $Ma = 4$ and the Hamaker number $A = 0.2$, as these values demonstrated increased flow instability in Fig. 2. Fig. 3a corresponds to the case of an exothermic chemical reaction ($X > 0$), while Fig. 3b represents the endothermic case ($X < 0$). The results reveal that an exothermic chemical reaction on

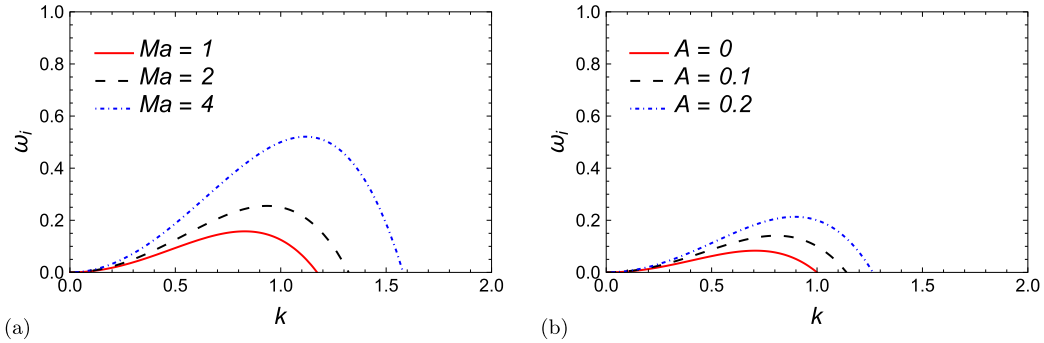

Fig. 2. Linear growth rate as a function of wavenumber k for different values of (a) Marangoni number Ma (when $A = 0$); (b) Hamaker number A (when $Ma = 0$) for $X = 0$ and $Bi = 1$.

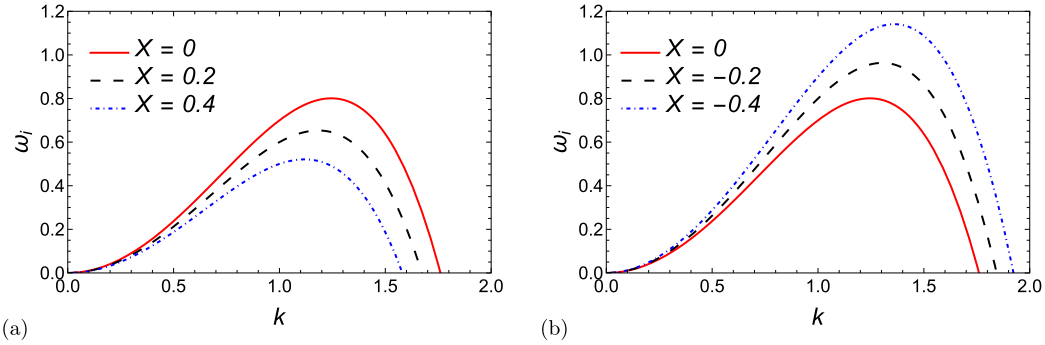

Fig. 3. Influence of the (a) exothermic reactions ($X > 0$); (b) endothermic reactions ($X < 0$) on the linear growth rate as a function of wavenumber k when $Ma = 4$, $A = 0.2$ and $Bi = 1$.

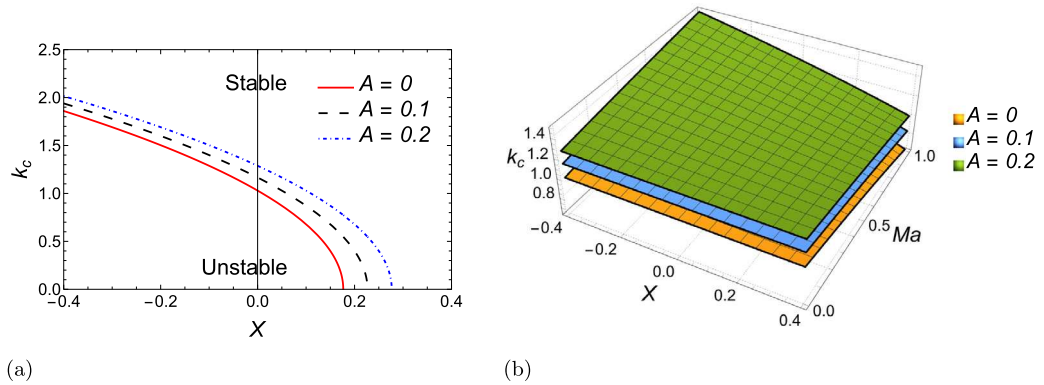

Fig. 4. Influence of the chemical reaction on the neutral stability curve for different values of A when $Ma = 4$ and $Bi = 0.01$.

the substrate inhibits instability, while an endothermic reaction intensifies it. Similar findings regarding the roles of exothermic and endothermic chemical reactions have also been reported by Chao et al. (2020) and Li and Chao (2020). We note that, despite the destabilizing effect of the combined van der Waals attraction and thermocapillary force, which intensifies the RP instability, Fig. 3 concludes that an exothermic reaction can alleviate it.

Fig. 4 depicts how van der Waals attractions affect the marginal stability curves in the $X - k$ plane for a heated vertical fiber. The unstable region in the $X - k$ plane expands with increasing Hamaker number A, indicating that van der Waals attraction has a destabilizing impact. Moreover, regardless of the presence or absence of A, the unstable region in the $X - k$ plane widens as the chemical reaction becomes more endothermic, i.e., as $X(< 0)$ values increase, and contracts as the reaction becomes more exothermic, i.e., as $X(> 0)$ values increase. This further validates the substantial stabilizing influence of an exothermic chemical reaction and underscores the destabilizing effect of an endothermic chemical reaction. In Fig. 4b, we present a three-dimensional view of the neutral stability curves to illustrate their variation with changes in both X and A.

To compare the result of the linear stability analysis from the present model and that reported by Ding et al. (2019) and Chao et al. (2020), we assume $\vartheta \propto \exp[\omega t + ikz]$. Considering Bi is small ($Bi \ll 1$) and Ma is large enough to retain the terms involving $MaBi$ (Chao et al., 2018), the dispersion relation can be derived as follows

$$\omega = -ik + k^2\left[\frac{1}{3}\left(1 - k^2\right) + A - \frac{MaX}{2} + M\right], \tag{23}$$

where $M = MaBi/2$ is the modified Marangoni number. Without van der Waals attractions, chemical reactions, and the modified Marangoni number M, the equation (23) exhibits a structure comparable to the one presented by Duprat et al. (2007). For $X = 0$, equation (23) matches with Ding et al. (2019) and for $A = 0$, it recovers Chao et al. (2020).

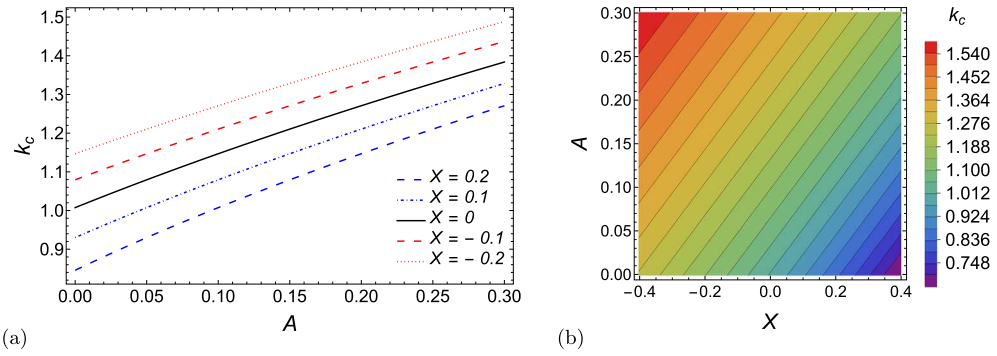

Fig. 5. (a) The impact of chemical reaction on the critical wavenumber (k_c) for various values of X. (b) Contour plot of k_c as a function of A and X. The other fixed parameters are $Ma = 1, Bi = 0.01$.

Further, we determine the value of k_c by substituting $\omega_r = 0$ in (23), leading to the expression

$$k_c = \sqrt{1 + 3(A + M) - 1.5MaX}. \tag{24}$$

Thus, the most unstable mode k_m can be obtained by evaluating $d\omega_r/dk = 0$ in (23), resulting in $k_m = \sqrt{0.5 + 1.5(A + M) - 0.75MaX}$. In the absence of a chemical reaction ($X = 0$), this expression for k_m aligns with Ding et al. (2019). When van der Waals attractions are absent ($A = 0$), and with $Ma = 1, Bi = 0.01$, we find $k_m = \sqrt{0.5075 - 0.75X}$, which matches the result obtained in Chao et al. (2020). It is evident that due to A and M being finite positive numbers, the values of k_c and, consequently, k_m will either increase or decrease depending on the increase of X (for $X < 0$) or X (for $X > 0$). Conversely, in the absence of a chemical reaction ($X = 0$), the values of k_c and, consequently, k_m will increase depending on the increase of both M and A. This behavior is illustrated in Fig. 5.

Considering $\alpha = 1$ in (18), with $\vartheta \propto \exp[\omega t + ikz]$, we obtain the dispersion relation as

$$\omega = -ik + k^2\left[\frac{1}{3Ca}\left(1 - k^2\right) + A - \frac{Ma(X - Bi)}{2(1 + Bi)^2}\right]. \tag{25}$$

We multiply (25) by i, and use the transformation $(i\omega, k) \to Ca^{1/3}\left(i\widetilde{\omega}, \widetilde{k}\right)$. Consequently, we obtain

$$\widetilde{\omega} = \widetilde{k} + \frac{i\widetilde{k}^2}{3}\left(\beta - \widetilde{k}^2\right), \tag{26}$$

where

$$\beta = Ca^{-2/3} + 3\left[A - \frac{Ma(X - Bi)}{2(1 + Bi)^2}\right]Ca^{1/3}. \tag{27}$$

This corresponds to the dispersion relation of a weakly nonlinear lubrication model studied by Frenkel (1992) excluding van der Waals attractions, thermocapillary effects, and chemical reactions. The standard dispersive relation (26) also mirrors those found by Duprat et al. (2007) and Ji et al. (2021). Duprat et al. (2007) determined the system's absolute instability when $\beta > \beta_c \equiv \left[(9/4) \times \left(-17 + 7\sqrt{7}\right)\right]^{1/3} \approx 1.507$. Consequently, for the present study, we obtain

$$A - \frac{Ma(X - Bi)}{2(1 + Bi)^2} > \frac{1}{3}\left[\frac{9}{4Ca}\left(-17 + 7\sqrt{7}\right)\right]^{1/3} - \frac{Ca^{-1}}{3}. \tag{28}$$

Moreover, if we consider $Bi \ll 1$, say $Bi = 0.01$ and Ma is large, say $Ma = 2$, then (28) shows

$$A > 0.16 + X \text{ (approx)}. \tag{29}$$

When $X = 0$, equation (29) corresponds to the condition established by Ding et al. (2019). Equation (29) indicates that when considering chemical reactions ($X \neq 0$), the absolute instability threshold depends on the nature of the reaction. For exothermic reactions ($X > 0$), the van der Waals attractions must exceed a higher value of A compared to a non-reactive liquid for instability to be absolute. Conversely, for endothermic reactions ($X < 0$), the van der Waals attractions need to exceed a lower value compared to a non-reactive liquid.

The above discussion revolves around linear stability, which provides only initial insights into the stability mechanism. We must consider nonlinear effects to understand how van der Waals attraction affects flow dynamics under chemical reactions and uniform heating. Therefore, this section will examine weakly nonlinear stability analysis (Desai et al., 2023; Jiang and Ding, 2022; Oron and Gottlieb, 2004) of the present model. We introduce small variables $z_1 = \varsigma z$, $t_1 = \varsigma t$, and $t_2 = \varsigma^2 t$, where $\varsigma \ll 1$ denotes the distance from criticality (Mukhopadhyay et al., 2019). We assume that the linear growth rate of the amplitude, denoted by ω_i, is of order $O(\varsigma^2)$. The resulting substitutions transform the partial derivatives as follows

$$\partial_t \to \partial_t + \varsigma\partial_{t_1} + \varsigma^2\partial_{t_2} + \cdots, \quad \partial_z \to \partial_z + \varsigma\partial_{z_1} + \varsigma^2\partial_{z_2} + \cdots. \tag{30}$$

We expand $\vartheta(z,t)$ as $\vartheta\left(z, z_1, z_2, \ldots, t, t_1, t_2\right) = \varsigma\vartheta_1 + \varsigma^2\vartheta_2 + \varsigma^3\vartheta_3 + \cdots$ and insert in (21) along with (30). This yields (Chattopadhyay and Ji, 2023; Jiang and Ding, 2022; Oron and Gottlieb, 2004; Sadiq and Usha, 2008)

$$\left(\mathcal{L}_0 + \varsigma\mathcal{L}_1 + \varsigma^2\mathcal{L}_2 + \cdots\right)\left(\varsigma\vartheta_1 + \varsigma^2\vartheta_2 + \varsigma^3\vartheta_3 + \cdots\right) = -\varsigma^2\mathcal{N}_2 - \varsigma^3\mathcal{N}_3 - \cdots, \tag{31}$$

where $\mathcal{L}_i$, $i = 0, 1, 2, \ldots$ are the operators and $\mathcal{N}_j$, $j = 2, 3, \ldots$ are the nonlinear terms. The explicit expressions of $\mathcal{L}_i$, $i = 0, 1, 2, \ldots$ and $\mathcal{N}_j$, $j = 2, 3, \ldots$ are given in Appendix B.

Solutions for ϑ_1 and ϑ_2 can be obtained by using different orders of ς. The solutions are as follows (Chattopadhyay and Ji, 2023; Jiang and Ding, 2022; Oron and Gottlieb, 2004; Sadiq and Usha, 2008)

$$\begin{aligned}\vartheta_1 &= \mathcal{E}\left(z_1, t_1, t_2\right)\exp\left[i\left(kz - \omega_r t\right)\right] + cc,\\ \vartheta_2 &= \frac{2k\left(\mathcal{F}' - \mathcal{T}'k^2\right) - i\mathcal{M}'}{4k\left(4\mathcal{T}k^2 - \mathcal{F}\right)}\mathcal{E}^2\exp\left[2i\left(kz - \omega_r t\right)\right] + cc,\end{aligned} \tag{32}$$

where $\mathcal{E} \ll 1$ is the disturbance amplitude.

Following Chattopadhyay (2021b); Chattopadhyay and Desai (2022); Chattopadhyay et al. (2022a); Mukhopadhyay et al. (2020), the complex Ginzburg-Landau equation (CGLE) is obtained as

$$\frac{\partial\mathcal{E}}{\partial t_2} + 2ik\left(\mathcal{F} - 2\mathcal{T}k^2\right)\varsigma^{-1}\frac{\partial\mathcal{E}}{\partial z_1} + \left(\mathcal{F} - 6\mathcal{T}k^2\right)\frac{\partial^2\mathcal{E}}{\partial z_1^2} - \varsigma^{-2}\omega_i\mathcal{E} + \left(R_2 + iR_4\right)|\mathcal{E}|^2\mathcal{E} = 0, \tag{33a}$$

$$R_2 = \frac{k^2}{2}\left(\mathcal{T}''k^2 - \mathcal{F}''\right) + \frac{(\mathcal{M}')^2 - 2k^2\left(\mathcal{F}' - 7\mathcal{T}'k^2\right)\left(\mathcal{F}' - \mathcal{T}'k^2\right)}{16\mathcal{T}k^2 - 4\mathcal{F}},$$

$$R_4 = \frac{1}{2}\mathcal{M}''k + \frac{3\mathcal{M}'\left(\mathcal{F}' - 3\mathcal{T}'k^2\right)k}{16\mathcal{T}k^2 - 4\mathcal{F}}. \tag{33b}$$

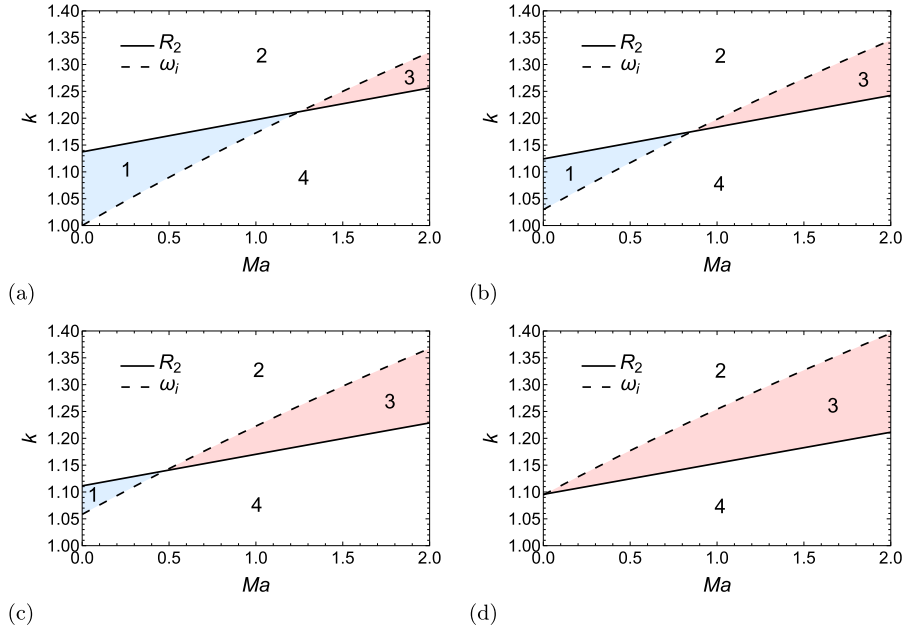

Fig. 6. Variation of k as a function of Marangoni number Ma for (a) $A = 0$; (b) $A = 0.02$; (c) $A = 0.04$; (d) $A = 0.066$ for $X = 0$ and $Bi = 1$.

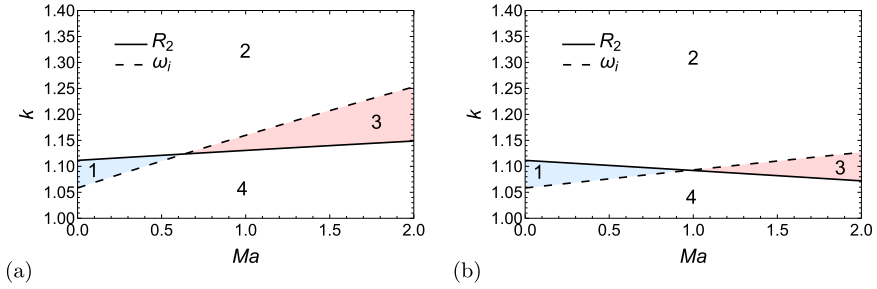

Fig. 7. Variation of k as a function of Marangoni number Ma for (a) $X = 0.4$; (b) $X = 0.8$ for $A = 0.04$ and $Bi = 1$.

The behavior of perturbation dynamics beyond the linear regime depends entirely on the sign of R_2, the Landau constant. Specifically, the sign of R_2 determines the stability of these dynamics. When $R_2 > 0$, the amplitude $\mathcal{E}$ saturates, indicating a supercritical bifurcation. Conversely, no saturation occurs when $R_2 < 0$, and this corresponds to a subcritical bifurcation (Oron and Gottlieb, 2004). If $R_2 = 0$, the resulting wave may be stable or unstable based on whether $\omega_i < 0$ or $\omega_i > 0$.

Based on the analysis, four stability zones have been identified and classified as follows: *"supercritical stable"* when $\omega_i < 0$ and $R_2 > 0$, *"subcritical stable"* when $\omega_i < 0$ and $R_2 < 0$, *"subcritical unstable"* when $\omega_i > 0$ and $R_2 < 0$, and *"supercritical unstable"* when $\omega_i > 0$ and $R_2 > 0$ (Sadiq and Usha, 2008; Sadiq et al., 2010). These four regions are denoted as zones 1, 2, 3, and 4. In Figs. 6-8, we visually elucidate the shifts in instability regions for a heated vertical fiber impacted by van der Waals attraction (regulated by the Hamaker number A) and exothermic reactions (indicated by $X > 0$) or endothermic reactions (denoted by $X < 0$) in the system.

Fig. 6 demonstrates the impact of van der Waals attraction on supercritical/subcritical zones 1 to 4 in the absence of any chemical reaction ($X = 0$). This is demonstrated by selecting four different values of the Hamaker number (A), i.e., $A = 0, 0.02$, and 0.04, depicted in Figs. 6a to 6c, respectively. The findings reveal that van der Waals attraction has a destabilizing effect on the flow system, as reflected by the reduction in the supercritical stable zone (zone 1) and the enlargement of the subcritical unstable zone (zone 3) with the increasing Hamaker number (A). Moreover, from Fig. 6d, it can be observed that the supercritical stable zone, where finite amplitude disturbances remain stable for both linear and nonlinear regimes, disappears at $A = A_c = 0.066$.

Fig. 7 illustrates the impact of an exothermic chemical reaction ($X > 0$) on supercritical/subcritical zones 1 to 4 under the influence of van der Waals attraction. The Hamaker number $A = 0.04$, which was used in Fig. 6c without any chemical reaction ($X = 0$) is kept fixed to show the effect of the exothermic chemical reaction. Two values of $X(> 0)$, specifically $X = 0.4$ and $X = 0.8$, are chosen for Figs. 7a and 7b, respectively. A comparison of Figs. 6c, 7a, and 7b reveal that the supercritical stable zone (zone 1) expands, while the subcritical unstable zone (zone 3) contracts as the value of X (> 0) increases. Thus, according to the findings presented in Fig. 7, while van der Waals attraction can exacerbate flow instability, an exothermic chemical reaction may serve as a means to mitigate this instability.

According to the results displayed in Fig. 8, the influence of van der Waals attraction on supercritical/subcritical zones 1 to 4 is examined in the presence of an endothermic chemical reaction ($X < 0$). The value of the Hamaker number A is fixed at 0.01, and two values of $X(< 0)$, namely $X = -0.4$ and $X = -0.8$, are chosen for Figs. 8a and 8b, respectively. Upon comparing Figs. 8a and 8b, it is evident that the supercritical stable zone (zone 1) contracts, while the subcritical unstable zone (zone 3) expands with an increase in the value of X (< 0). Thus, the findings suggest that van der Waals attraction can aggravate flow instability, while an endothermic chemical reaction can intensify it.

To obtain a solution for (33), we consider those waves in which spatial modulation does not exist (filtered wave) and consequently (33) reduces to

$$\frac{\partial \mathcal{E}}{\partial t_2} - \varsigma^{-2}\omega_i \mathcal{E} + \left(R_2 + iR_4\right)|\mathcal{E}|^2 \mathcal{E} = 0. \tag{34}$$

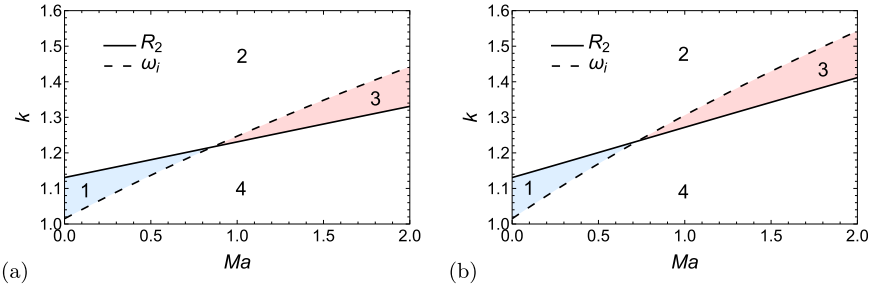

Fig. 8. Variation of k as a function of Marangoni number Ma for (a) $X = -0.4$; (b) $X = -0.8$ for $A = 0.01$ and $Bi = 1$.

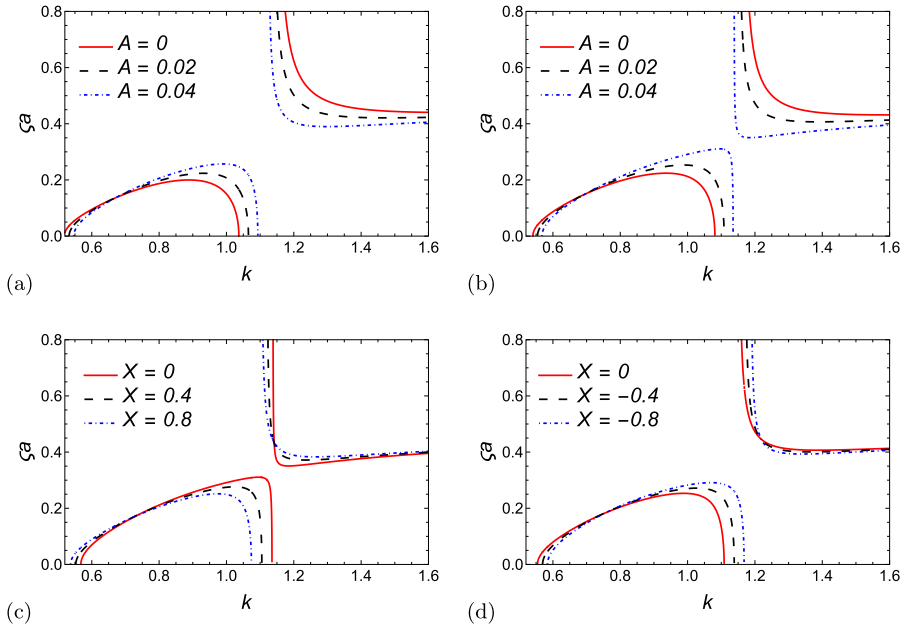

Fig. 9. Threshold amplitude (ςa) variation with wavenumber (k) in supercritical unstable and subcritical stable zones for different parameter combinations: (a) $X = 0$, $Ma = 0.2$; (b) $X = 0$, $Ma = 0.45$; (c) $A = 0.04$, $Ma = 0.45$; (d) $A = 0.02$, $Ma = 0.45$, with $Bi = 1$.

For a filtered wave, $\mathcal{E}$ can be written as $\mathcal{E} = a\left(t_2\right) e^{-i\xi\left(t_2\right)t_2}$ (Jiang and Ding, 2022; Mukhopadhyay and Chattopadhyay, 2018; Mukhopadhyay et al., 2020). Consequently, inserting $\mathcal{E}$ in (34) leads to a nonlinear ODE for a as follows:

$$\frac{da}{dt_2} - ia\frac{d\left(\xi\left(t_2\right)t_2\right)}{dt_2} - \varsigma^{-2}\omega_i a + \left(R_2 + iR_4\right)a^3 = 0. \tag{35}$$

Further, we separate the real and imaginary parts of (35). The real part gives

$$\frac{da}{dt_2} = \varsigma^{-2}\omega_i a - R_2 a^3. \tag{36}$$

For $a \neq 0$ and independent of t_2, equation (36) yields the threshold amplitude for the filtered wave as (Chattopadhyay et al. (2021); Sadiq and Usha (2008))

$$\varsigma a = \sqrt{\frac{\omega_i}{R_2}}. \tag{37}$$

Fig. 9 illustrates the sensitivity of the threshold amplitude to van der Waals attraction, both with and without a chemical reaction. Without a chemical reaction ($X = 0$), increasing the Hamaker number A raises the threshold amplitude in the supercritical unstable zone (zone 4) and lowers it in the subcritical stable zone (zone 2), with a stronger Marangoni effect amplifying these changes (Figs. 9a, 9b). In the presence of van der Waals attraction ($A = 0.04$), an exothermic reaction ($X > 0$) reduces the threshold amplitude in zone 4 and increases it in zone 2 (Fig. 9c), while an endothermic reaction ($X < 0$) has the opposite effect, increasing the threshold amplitude in zone 4 and decreasing it in zone 2 (Fig. 9d).

4. Numerical simulations

To comprehensively examine the growth of film instability considering the thermocapillary effect, van der Waals attractions, and chemical reaction, it is necessary to consider the complete nonlinear evolution equation as given in (19). For computations, we adopt a finite periodic domain with $0 \leq z < L$, where $L = 2\pi/k$ represents the length of the computational domain. We set the initial condition as

$$H(z,0) = 1 + 0.1\sin(kz). \tag{38}$$

To numerically simulate the solution for equation (19), a truncated Fourier series is employed, given by $H(z,t) = \sum_{-(N/2)+1}^{N/2} \widehat{H}_n \exp(inkz)$. Here, $\widehat{H}_n$ represents the Fourier amplitude of the perturbations. Following Chattopadhyay et al. (2022b), we conduct a convergence study for the current study that indicates $N = 2^8$ and $\Delta t = 0.01$ provide sufficiently accurate solutions for the numerical simulations. The analysis focuses on the film's evolution within the supercritical stability region. In Figs. 10 to 12, we set $k = 0.8$ and use a relative error tolerance of 10^{-6}.

Fig. 10 illustrates the influence of van der Waals attractions on the dynamics of a thin film flowing down a vertical fiber without any chemical reaction, specifically when $X = 0$. To investigate this phenomenon, three representative values of the Hamaker number A ($A = 0, 0.02, 0.04$)

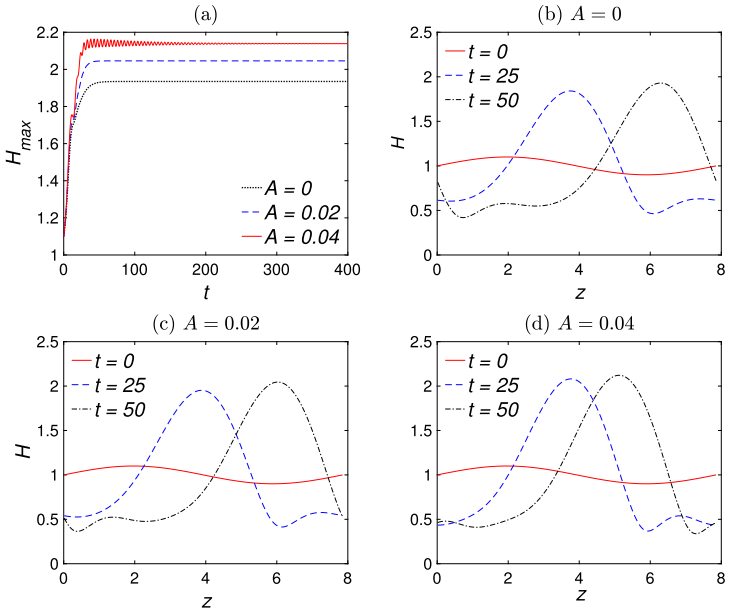

Fig. 10. Influence of van der Waals attractions. (a) Maximum (H_{max}) amplitude of the film thickness for different A; (b)-(d) Temporal evolution of the film profiles. The other fixed parameters are $X = 0$, $Ma = 2$, $Bi = 1$.

are selected to measure the strength of van der Waals attractions. Fig. 10a depicts the evolution of the maximum thickness. We find that the disturbance amplitude (H_{max}) increases with increasing A. In all presented cases, the disturbances experience initial growth, reaching a peak value, before eventually transitioning into a steady state over a more extended period. While the general trend remains similar across the cases, the wave amplitude exhibits rapid evolution with slight oscillations as A increases. By comparing the wave amplitudes, it becomes evident that van der Waals attractions destabilize the film dynamics, leading to an amplified wave amplitude growth. This observed effect becomes more prominent as A increases. The temporal evolution of film profiles at specific times ($t = 0, 25, 50$) is shown in Figs. 10b to 10d, both with and without A. Comparing these subfigures reveals that at any given time t, interfacial waves exhibit larger peaks with increasing values of A.

Fig. 11 shows the dynamics of the film on the fiber with van der Waals attractions and an exothermic chemical reaction ($X > 0$). We display the results for $A = 0.04$ as we observed oscillations in the absence of a chemical reaction ($X = 0$) for this specific value of A in Fig. 10a. The parameters other than A remain consistent with those in Fig. 10. In Fig. 11a, the maximum thickness evolution over time is depicted, revealing that increasing the parameter X leads to a decrease in disturbance amplitude (H_{max}). Across all scenarios presented, disturbances initially grow to a peak value before stabilizing over time. A comparison of the wave amplitudes reveals that exothermic chemical reactions exert a stabilizing influence on the dynamics of the film, resulting in a reduced amplification of the wave amplitude. This observed effect becomes more pronounced with higher values of X (where $X > 0$). Film profiles at $t = 25$ and $t = 50$ are shown in Figs. 11b and 11c, respectively, illustrating temporal changes influenced by the Hamaker number A. These subfigures demonstrate that stronger exothermic reactions lead to smaller peaks in interfacial waves. In summary, Fig. 11 underscores the stabilizing influence of exothermic chemical reactions in mitigating instability induced by van der Waals attraction.

Fig. 12 illustrates the dynamics of the film flowing down the fiber under the influence of van der Waals attractions and an endothermic chemical reaction ($X < 0$). Here also we set $A = 0.04$ as Fig. 11. The parameters other than A remain unchanged and consistent with those in Fig. 10. In Fig. 12, the evolution of maximum thickness over time is depicted, indicating that increasing the parameter X (where $X < 0$)

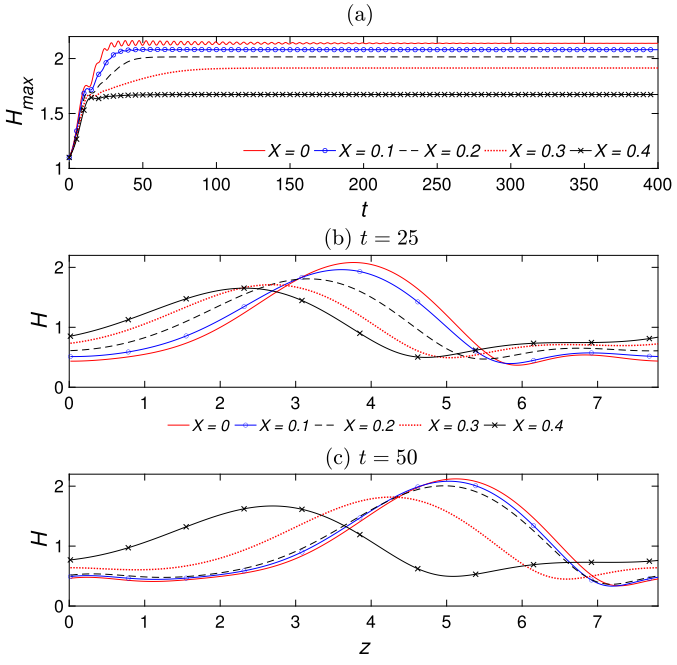

Fig. 11. Influence of exothermic reactions ($X > 0$). (a) Maximum (H_{max}) amplitude of the film thickness for different X; (b)-(c) Temporal evolution of the film profiles. The other fixed parameters are $A = 0.04$, $Ma = 2$, $Bi = 1$.

intensifies the disturbance amplitude (H_{max}). While the overall trend remains consistent across all scenarios, the magnitude of oscillations observed in the absence of a chemical reaction ($X = 0$) notably increases with higher values of X (where $X < 0$). Comparing wave amplitudes, it becomes evident that endothermic chemical reactions destabilize the film dynamics, leading to increased wave amplification. This effect becomes more pronounced as higher negative values of X are considered.

To study the influence of chemical reaction on the breakup phenomena, we set $k = 0.1$ and choose the initial condition as Matar et al. (2007)

$$H(z,0) = 1 + 0.01\exp\left[-0.5\,(z-10)^2\right] \tag{39}$$

and the corresponding plots are shown in Figs. 13 and 14. In Fig. 13a,

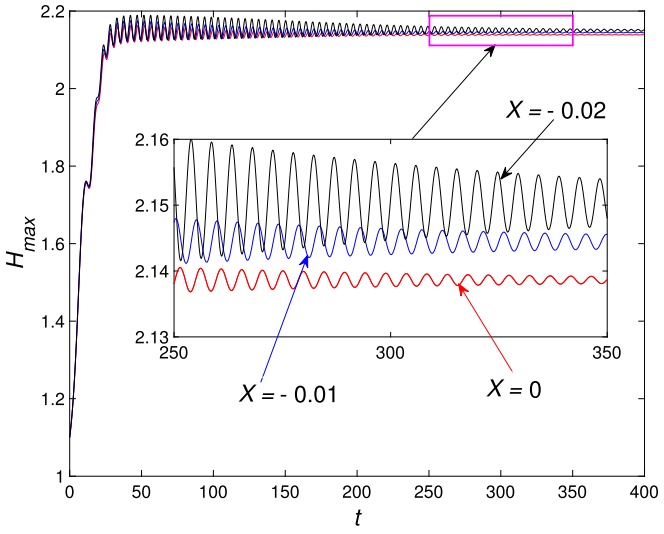

Fig. 12. Influence of endothermic reactions ($X < 0$) on the maximum (H_{max}) amplitude of the film thickness for $A = 0.04$, $Ma = 2$, $Bi = 1$.

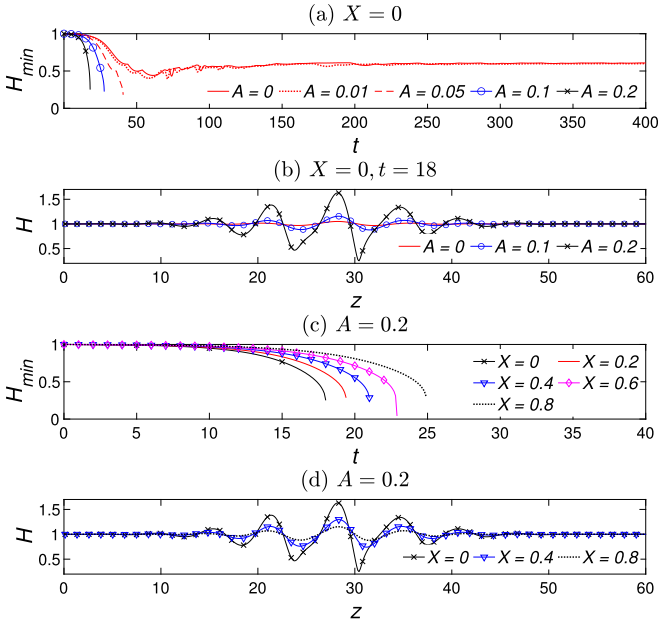

Fig. 13. (a,c) The minimum thickness (H_{min}); (b,d) Film profiles (at $t = 18$) for different A and exothermic reactions ($X > 0$) when $Ma = 1$, $Bi = 1$.

we illustrate the evolution of minimum amplitude profiles (H_{min}) without any chemical reaction ($X = 0$) for different values of A. The figure demonstrates that a stronger van der Waals attraction leads to a more rapid reduction in H_{min}. Based on Fig. 13a, we focus on the time $t = 18$ to visualize free surface configurations for the same A values selected earlier. We observe as A increases, the surface wave instability becomes more pronounced. To investigate the impact of exothermic chemical reactions (i.e., when $X > 0$), we set A to a constant value of 0.2 and select three distinct values of X, namely $X = 0$, $X = 0.4$, and $X = 0.8$. By comparing Figs. 13a and 13c, it becomes evident that a higher value of $X > 0$ delays the decrease of H_{min}. As a result, we plot the free surface configurations for $A = 0.2$ and the three aforementioned X values ($X = 0$, $X = 0.4$, and $X = 0.8$) at $t = 18$ in Fig. 13d. Further comparison between Figs. 13b and 13d reveals that increasing X (> 0) significantly reduces the surface wave instability. Therefore, the overall conclusion drawn from Fig. 13 is that although the combined effect of van der Waals attraction (via A) and heating ($Ma = 1$) promotes surface wave instability, the presence of an exothermic chemical reaction and its higher values can effectively suppress this surface wave instability.

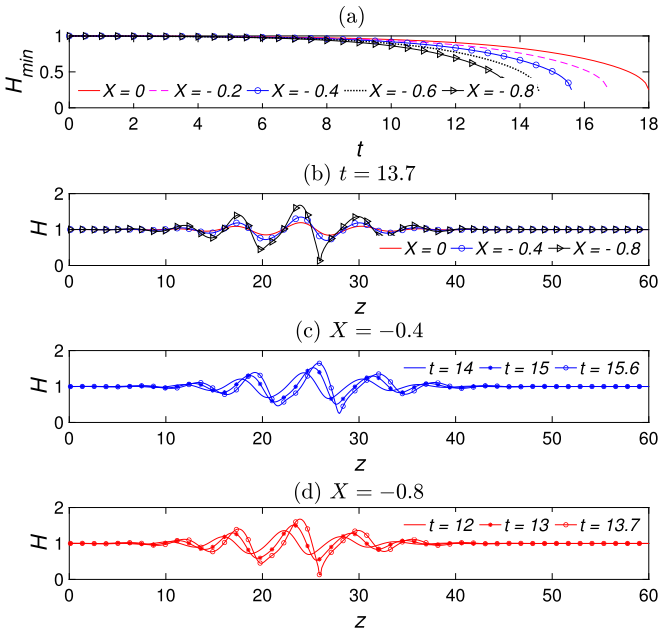

Fig. 14. (a) The minimum thickness (H_{min}); (b,c,d) Film profiles at different time t for endothermic reactions ($X < 0$) when $A = 0.2$, $Ma = 1$, $Bi = 1$.

Fig. 14 depicts the impact of an endothermic chemical reaction ($X < 0$) in the presence of van der Waals attraction ($A = 0.2$) and thermal effects ($Ma = 1$). In Fig. 14a, we show the evolution of minimum amplitude profiles (H_{min}) for various values of $X < 0$. It is evident from the figure that larger negative values of X result in a more rapid reduction in H_{min}, indicating a stronger effect of the endothermic reaction. To investigate this behavior further, we focus on a specific time, $t = 13.5$, and visualize Fig's corresponding free surface configurations. As shown in Fig. 14b, an increase in the magnitude of $X < 0$ leads to a more pronounced surface wave instability. Therefore, the top panel of Fig. 14 concludes that surface wave instability is more significant when an endothermic reaction is present than the scenario without any chemical reaction. Figs. 14c and 14d display the temporal evolutions of the film profiles captured at sequential times, specifically $t = 14, 15, 15.6$ for $X = -0.4$, and $t = 12, 13, 13.7$ for $X = -0.8$, respectively. These figures reveal that for a constant value of X (< 0), the interfacial waves exhibit higher humps as time progresses.

5. Summary and conclusions

This study analyzes the dynamic behavior of reactive ultra-thin liquid films as they flow along heated vertical fibers. The investigation focuses on the interplay among several crucial factors, including the influence of pseudo-zero-order exothermic or endothermic chemical reactions and the proportional effects of van der Waals attractions, which vary with h^{-3}. By assuming that the thickness of the liquid film is significantly smaller than the radius of the fiber, a nonlinear partial differential equation is derived to describe the evolution of the thin film. The linear stability of the system is examined through a thorough exploration of the resulting thin-film equation. The analysis reveals that van der Waals attractions play a critical role in augmenting the overall instability of the system. Importantly, it is observed that even in the presence of these attractions, an exothermic reaction contributes an additional stabilizing effect, whereas an endothermic reaction leads to the destabilization of the system. Moreover, by employing weakly nonlinear stability analysis, the study predicts the existence of distinct regions within the system. These regions include supercritical and subcritical regions, further emphasizing the multifaceted nature of the phenomenon. To investigate

the nonlinear evolution of the film thickness, we numerically solve the evolution equation within a periodic domain. The obtained results from these simulations corroborate the findings derived from the linear and weakly nonlinear stability analyses, confirming their validity and reliability.

This study explores how non-isothermal chemical reactions, when combined with van der Waals attractions, affect the dynamic behavior of thin liquid films flowing along vertical fibers. These results are expected to motivate the design of more efficient and optimized processes for engineering systems involving thin liquid films in non-isothermal environments.

CRediT authorship contribution statement

Souradip Chattopadhyay: Writing – original draft, Visualization, Validation, Software, Methodology, Investigation, Formal analysis, Conceptualization. **Hangjie Ji:** Writing – review & editing, Validation, Supervision, Project administration, Investigation, Funding acquisition, Formal analysis, Conceptualization.

Declaration of competing interest

The authors declare the following financial interests/personal relationships which may be considered as potential competing interests: Hangjie Ji reports financial support was provided by National Science Foundation. If there are other authors, they declare that they have no known competing financial interests or personal relationships that could have appeared to influence the work reported in this paper.

Data availability

Data will be made available on request.

Declaration of generative AI and AI-assisted technologies in the writing process

During the preparation of this work, the authors used ChatGPT in order to improve the language and readability of the article. After using this tool, the authors reviewed and edited the content as needed and take full responsibility for the content of the publication.

Acknowledgements

H.J. acknowledges support from NSF DMS 2309774. We sincerely thank the chief editor and anonymous referees for their valuable suggestions and insightful comments, which have significantly improved the quality of this manuscript.

Appendix A. Dimensional system of equations

The dynamics of the liquid film along the outer surface of the heated cylinder is governed by the continuity, Navier-Stokes, energy, and mass transport of reactants, which are presented below (Chao et al., 2020; Chattopadhyay, 2023; Trevelyan and Kalliadasis, 2004a; Trevelyan et al., 2002)

$$r^{-1}(ru_1)_r + u_{2,z} = 0, \tag{40a}$$

$$\rho\left(u_{1,t} + u_1u_{1,r} + u_2u_{2,z}\right) = -p_r + \mu\left[r^{-1}\left(ru_{1,r}\right)_r - u_1r^{-2} + u_{1,zz}\right], \tag{40b}$$

$$\rho\left(u_{2,t} + u_1u_{2,r} + u_2u_{2,z}\right) = -p_z + \rho g + \mu\left[r^{-1}\left(ru_{2,r}\right)_r + u_{2,zz}\right], \tag{40c}$$

$$T_t + u_1T_r + u_2T_z = \kappa\left[r^{-1}\left(rT_r\right)_r + T_{zz}\right] + bY\varkappa, \tag{40d}$$

$$\varkappa_t + u_1\varkappa_r + u_2\varkappa_z = d_{\mathrm{mol}}\left[r^{-1}\left(r\varkappa_r\right)_r + \varkappa_{zz}\right] - b\varkappa, \tag{40e}$$

where ρ is the liquid density, p is the pressure of the species $\mathcal{Z}_1$, μ is the dynamic viscosity, g is the gravitational acceleration, T is the temperature of the species $\mathcal{Z}_1$, κ is the thermal diffusivity, b is the reaction rate, Y is the heat release or consumption, $\varkappa$ is the concentration of the species $\mathcal{Z}_1$, and d_{mol} is the molecular diffusivity of the species $\mathcal{Z}_1$ and (u_1, u_2) the radial (r) and axial (z) velocity components.

At the cylinder wall $r = R$, we impose the following boundary conditions: no-slip and no penetration for velocity, uniform heating for thermal conditions, and a no-flux condition for species (Chao et al., 2020; Li and Chao, 2020; Trevelyan et al., 2002):

$$u_1 = 0, \quad u_2 = 0, \quad T = T_s, \quad \varkappa_r = 0, \tag{40f}$$

where T_s denotes the temperature at the cylinder surface.

The boundary conditions on the liquid-air interface $r = R + h(z,t)$ are the stress balances (along tangential and normal directions), kinematic condition, and Newton's law of cooling (Chao et al., 2018; Chattopadhyay, 2021a; Kalliadasis et al., 2012). In addition, a constant concentration of species $\mathcal{Z}_1$ is imposed at the liquid-air interface following Li and Chao (2020); Trevelyan and Kalliadasis (2004a); Trevelyan et al. (2002). These conditions are given below:

$$\mu\left[\left(u_{1,z} + u_{2,r}\right)\left(1 - h_z^2\right) + 2\left(u_{1,r} - u_{2,z}\right)h_z\right] = \left(\sigma_z + h_z\sigma_r\right)\left(1 + h_z^2\right)^{1/2}, \tag{40g}$$

$$\frac{A'}{h^3} + p_\infty - p + 2\mu\left[u_{1,r} + u_{2,z}h_z^2 - \left(u_{1,z} + u_{2,r}\right)h_z\right]\left(1 + h_z^2\right)^{-1} = -\sigma(T)\left[\left(1 + h_z^2\right)r^{-1} - h_{zz}\right]\left(1 + h_z^2\right)^{-3/2}, \tag{40h}$$

$$u_1 = h_t + u_2h_z, \tag{40i}$$

$$\lambda\left(T_r - h_zT_z\right)\left(1 + h_z^2\right)^{-1/2} + k_g\left(T - T_\infty\right) = 0, \tag{40j}$$

$$\varkappa = C, \tag{40k}$$

where σ is the surface tension, p_∞ is the atmospheric pressure, λ is the thermal conductivity, k_g is the heat transfer coefficient of the liquid, C represents the initial concentration of the species $\mathcal{Z}_1$. In (40h), A' represents the dimensional Hamaker constant. We assume $A' > 0$, indicating a destabilizing van der Waals force. To model the breakup process, the van der Waals attractions are assumed to vary proportionally to h^{-3} (Burelbach et al., 1988).

Appendix B. Explicit expressions of $\mathcal{L}_i$, $i = 0, 1, 2, \ldots$ and $\mathcal{N}_j$, $j = 2, 3, \ldots$ in (31)

$$\mathcal{L}_0 \equiv \frac{\partial}{\partial t} + \mathcal{M}\frac{\partial}{\partial z} + \mathcal{F}\frac{\partial^2}{\partial z^2} + \mathcal{T}\frac{\partial^4}{\partial z^4},$$

$$\mathcal{L}_1 \equiv \frac{\partial}{\partial t_1} + \mathcal{M}\frac{\partial}{\partial z_1} + 2\mathcal{F}\frac{\partial^2}{\partial z\partial z_1} + 4\mathcal{T}\frac{\partial^4}{\partial z^3\partial z_1},$$

$$\mathcal{L}_2 \equiv \frac{\partial}{\partial t_2} + \mathcal{F}\frac{\partial^2}{\partial z_1^2} + 6\mathcal{T}\frac{\partial^4}{\partial z^2\partial z_1^2},$$

$$\mathcal{N}_2 \equiv \mathcal{M}'\vartheta_1\frac{\partial\vartheta_1}{\partial z} + \mathcal{F}'\left[\vartheta_1\frac{\partial^2\vartheta_1}{\partial z^2} + \left(\frac{\partial\vartheta_1}{\partial z}\right)^2\right] + \mathcal{T}'\left[\vartheta_1\frac{\partial^4\vartheta_1}{\partial z^4} + \frac{\partial\vartheta_1}{\partial z}\frac{\partial^3\vartheta_1}{\partial z^3}\right],$$

$$\mathcal{N}_3 \equiv \mathcal{M}'\left[\vartheta_1\left(\frac{\partial\vartheta_2}{\partial z} + \frac{\partial\vartheta_1}{\partial z_1}\right) + \vartheta_2\frac{\partial\vartheta_1}{\partial z}\right]$$
$$+\mathcal{F}'\left[\vartheta_1\left(\frac{\partial^2\vartheta_2}{\partial z^2} + 2\frac{\partial^2\vartheta_1}{\partial z\partial z_1}\right) + \vartheta_2\frac{\partial^2\vartheta_1}{\partial z^2} + 2\frac{\partial\vartheta_1}{\partial z}\left(\frac{\partial\vartheta_2}{\partial z} + \frac{\partial\vartheta_1}{\partial z_1}\right)\right]$$
$$+\mathcal{T}'\left[\vartheta_1\left(\frac{\partial^4\vartheta_2}{\partial z^4} + 4\frac{\partial^4\vartheta_1}{\partial z^3\partial z_1}\right) + \vartheta_2\frac{\partial^4\vartheta_1}{\partial z^4} + \frac{\partial\vartheta_1}{\partial z}\left(\frac{\partial^3\vartheta_2}{\partial z^3} + 3\frac{\partial^3\vartheta_1}{\partial z^2\partial z_1}\right)\right.$$
$$\left. + \frac{\partial^3\vartheta_1}{\partial z^3}\left(\frac{\partial\vartheta_2}{\partial z} + \frac{\partial\vartheta_1}{\partial z_1}\right)\right]$$
$$+\frac{1}{2}\mathcal{M}''\vartheta_1^2\frac{\partial\vartheta_1}{\partial z} + \mathcal{F}''\left(\frac{1}{2}\vartheta_1^2\frac{\partial^2\vartheta_1}{\partial z^2} + \vartheta_1\left(\frac{\partial\vartheta_1}{\partial z}\right)^2\right)$$
$$+\mathcal{T}''\left(\frac{1}{2}\vartheta_1^2\frac{\partial^4\vartheta_1}{\partial z^4} + \vartheta_1\frac{\partial\vartheta_1}{\partial z}\frac{\partial^3\vartheta_1}{\partial z^3}\right).$$

References

Bertozzi, A.L., Pugh, M.C., 1998. Long-wave instabilities and saturation in thin film equations. Commun. Pure Appl. Math. 51, 625–661.

Biswal, S., Ji, H., Elamvazhuthi, K., Bertozzi, A.L., 2024. Optimal boundary control of a model thin-film fiber coating model. Phys. D, Nonlinear Phenom. 457, 133942.

Braun, R.J., Murray, B.T., Boettinger, W.J., McFadden, G.B., 1995. Lubrication theory for reactive spreading of a thin drop. Phys. Fluids 7, 1797–1810.

Burelbach, J.P., Bankoff, S.G., Davis, S.H., 1988. Nonlinear stability of evaporating/condensing liquid films. J. Fluid Mech. 195, 463–494.

Chao, Y., Ding, Z., Liu, R., 2018. Dynamics of thin liquid films flowing down the uniformly heated/cooled cylinder with wall slippage. Chem. Eng. Sci. 175, 354–364.

Chao, Y., Lu, Y., Yuan, H., 2020. On reactive thin liquid films falling down a vertical cylinder. Int. J. Heat Mass Transf. 147, 118942.

Chattopadhyay, S., 2021a. Thermocapillary instability in the presence of uniform normal electric field: effect of odd viscosity. J. Eng. Math. 131, 1–22.

Chattopadhyay, S., 2021b. Odd-viscosity-induced instability of a thin film with variable density. Phys. Fluids 33, 082102.

Chattopadhyay, S., 2023. Thin liquid films on a slippery vertical cylinder in presence of chemical reaction. Chem. Eng. Sci. 282, 119211.

Chattopadhyay, S., 2024. Falling liquid film down a non-uniformly heated slippery inclined plane with odd viscosity effects. Int. J. Heat Mass Transf. 218, 124807.

Chattopadhyay, S., Desai, A.S., 2022. Dynamics and stability of weakly viscoelastic film flowing down a uniformly heated slippery incline. Phys. Rev. Fluids 7, 064007.

Chattopadhyay, S., Ji, H., 2023. Thermocapillary thin film flows on a slippery substrate with odd viscosity effects. Phys. D: Nonlinear Phenom. 455, 133883.

Chattopadhyay, S., Mukhopadhyay, A., Barua, A.K., Gaonkar, A.K., 2021. Thermocapillary instability on a film falling down a non-uniformly heated slippery incline. Int. J. Non-Linear Mech. 133, 103718.

Chattopadhyay, S., Boragunde, P., Gaonkar, A.K., Barua, A.K., Mukhopadhyay, A., 2022a. Falling liquid films on a slippery substrate with variable fluid properties. Int. J. Non-Linear Mech. 147, 104200.

Chattopadhyay, S., Subedar, G.Y., Gaonkar, A.K., Barua, A.K., Mukhopadhyay, A., 2022b. Effect of odd-viscosity on the dynamics and stability of a thin liquid film flowing down on a vertical moving plate. Int. J. Non-Linear Mech. 140, 103905.

Craster, R., Matar, O.K., 2009. Dynamics and stability of thin liquid films. Rev. Mod. Phys. 81, 1131–1198.

Craster, R.V., Matar, O.K., 2006. On viscous beads flowing down a vertical fibre. J. Fluid Mech. 553, 85–105.

Dagan, Z., Pismen, L.M., 1984. Marangoni waves induced by a multistable chemical reaction on thin liquid films. J. Colloid Interface Sci. 99, 215–225.

Dagaut, P., Pengloan, G., Ristori, A., 2002. Oxidation, ignition and combustion of toluene: experimental and detailed chemical kinetic modeling. Phys. Chem. Chem. Phys. 4, 1846–1854.

Dávalos-Orozco, L.A., You, X., 2000. Three-dimensional instability of a liquid layer flowing down a heated vertical cylinder. Phys. Fluids 12, 2198–2209.

Desai, A.S., Chattopadhyay, S., Gaonkar, A.K., 2023. Shear imposed falling liquid films on a slippery substrate with Marangoni effects: effect of odd viscosity. Int. J. Non-Linear Mech. 156, 104507.

Ding, Z., Wong, T.N., 2017. Three-dimensional dynamics of thin liquid films on vertical cylinders with Marangoni effect. Phys. Fluids 29, 011701.

Ding, Z., Liu, R., Wong, T.N., Yang, C., 2018. Absolute instability induced by Marangoni effect in thin liquid film flows on vertical cylindrical surfaces. Chem. Eng. Sci. 177, 261–269.

Ding, Z., Liu, Z., Liu, R., Yang, C., 2019. Breakup of ultra-thin liquid films on vertical fiber enhanced by Marangoni effect. Chem. Eng. Sci. 199, 342–348.

Duprat, C., Ruyer-Quil, C., Kalliadasis, S., Giorgiutti-Dauphiné, F., 2007. Absolute and convective instabilities of a viscous film flowing down a vertical fiber. Phys. Rev. Lett. 98, 244502.

Frenkel, A.L., 1992. Nonlinear theory of strongly undulating thin films flowing down vertical cylinders. Europhys. Lett. 18, 583.

Gallez, D., De Wit, A., Kaufman, M., 1996. Dynamics of a thin liquid film with a surface chemical reaction. J. Colloid Interface Sci. 180, 524–536.

Hatziavramidis, D., 1992. Stability of thin evaporating/condensing films in the presence of surfactants. Int. J. Multiph. Flow 18, 517–530.

Herminghaus, S., Jacobs, K., Mecke, K., Bischof, J., Fery, A., Ibn-Elhaj, M., Schlagowski, S., 1998. Spinodal dewetting in liquid crystal and liquid metal films. Science 282, 916–919.

Ji, H., Falcon, C., Sadeghpour, A., Zeng, Z., Ju, Y.S., Bertozzi, A.L., 2019. Dynamics of thin liquid films on vertical cylindrical fibres. J. Fluid Mech. 865, 303–327.

Ji, H., Falcon, C., Sedighi, E., Sadeghpour, A., Ju, Y.S., Bertozzi, A.L., 2021. Thermally-driven coalescence in thin liquid film flowing down a fibre. J. Fluid Mech. 916, A19.

Jiang, W., Ding, Z., 2022. Thin liquid films down a vertical microfiber: effect of curvature elasticity. Phys. Rev. E 105, 035104.

Kalliadasis, S., Chang, H.C., 1994. Drop formation during coating of vertical fibres. J. Fluid Mech. 261, 135–168.

Kalliadasis, S., Ruyer-Quil, C., Scheid, B., Velarde, M.G., 2012. Falling Liquid Films. Applied Mathematical Sciences, vol. 176. Springer.

Kim, B., Ji, H., Bertozzi, A.L., Sadeghpour, A., Ju, Y.S., 2024. A positivity-preserving numerical method for a thin liquid film on a vertical cylindrical fiber. J. Comput. Phys. 496, 112560.

Kliakhandler, I.L., Davis, S.H., Bankoff, S.G., 2001. Viscous beads on vertical fibre. J. Fluid Mech. 429, 381–390.

Kundan, A., Nguyen, T.T.T., Plawsky, J.L., Wayner Jr., P.C., Chao, D.F., Sicker, R.J., 2017. Condensation on highly superheated surfaces: unstable thin films in a wickless heat pipe. Phys. Rev. Lett. 118, 094501.

Li, P., Chao, Y., 2020. Marangoni instability of self-rewetting films modulated by chemical reactions flowing down a vertical fibre. Chem. Eng. Sci. 227, 115936.

Lister, J.R., Rallison, J.M., King, A.A., Cummings, L.J., Jensen, O.E., 2006. Capillary drainage of an annular film: the dynamics of collars and lobes. J. Fluid Mech. 552, 311–343.

Liu, R., Liu, Q.S., 2014. Thermocapillary effect on the dynamics of viscous beads on vertical fiber. Phys. Rev. E 90, 033005.

Matar, O.K., 2002. Nonlinear evolution of thin free viscous films in the presence of soluble surfactant. Phys. Fluids 14, 4216–4234.

Matar, O.K., Spelt, P.D.M., 2005. Dynamics of thin free films with reaction-driven density and viscosity variations. Phys. Fluids 17, 122102.

Matar, O.K., Craster, R.V., Kumar, S., 2007. Falling films on flexible inclines. Phys. Rev. E 76, 056301.

Mukhopadhyay, A., Chattopadhyay, S., 2018. Long wave instability of thin film flowing down an inclined plane with linear variation of thermophysical properties for very small Biot number. Int. J. Non-Linear Mech. 100, 20–29.

Mukhopadhyay, A., Chattopadhyay, S., Barua, A.K., 2019. Stability of thin liquid film flowing down a rotating horizontal or inclined plane by momentum-integral method. Eur. J. Mech. B, Fluids 75, 58–70.

Mukhopadhyay, A., Chattopadhyay, S., Barua, A.K., 2020. Stability of thin film flowing down the outer surface of a rotating non-uniformly heated vertical cylinder. Nonlinear Dyn. 100, 1143–1172.

Norinaga, K., Deutschmann, O., 2007. Detailed kinetic modeling of gas-phase reactions in the chemical vapor deposition of carbon from light hydrocarbons. Ind. Eng. Chem. Res. 46, 3547–3557.

Oron, A., Gottlieb, O., 2004. Subcritical and supercritical bifurcations of the first- and second-order Benney equations. J. Eng. Math. 50, 121–140.

Oron, A., Davis, S.H., Bankoff, S.G., 1997. Long-scale evolution of thin liquid films. Rev. Mod. Phys. 69, 931–980.

Pereira, A., Trevelyan, P.M.J., Thiele, U., Kalliadasis, S., 2007. Interfacial hydrodynamic waves driven by chemical reactions. J. Eng. Math. 59, 207–220.

Petrucci, R.H., 2017. General Chemistry: Principles and Modern Applications. Pearson.

Quéré, D., 1990. Thin films flowing on vertical fibers. Europhys. Lett. 13, 721–726.

Quéré, D., 1999. Fluid coating on a fiber. Annu. Rev. Fluid Mech. 31, 347–384.

Rayleigh, L., 1892. On the instability of a cylinder of viscous liquid under capillary force. Lond. Edinb. Dublin Philos. Mag. J. Sci. 34, 145–154.

Reisfeld, B., Bankoff, S.G., 1992. Non-isothermal flow of a liquid film on a horizontal cylinder. J. Fluid Mech. 236, 167–196.

Ruckenstein, E., Jain, R.K., 1974. Spontaneous rupture of thin liquid films. J. Chem. Soc., Faraday Trans. 2: Mol. Chem. Phys. 70, 132–147.

Ruyer-Quil, C., Treveleyan, P., Giorgiutti-Dauphiné, F., Duprat, C., Kalliadasis, S., 2008. Modelling film flows down a fibre. J. Fluid Mech. 603, 431–462.

Sadiq, I.M.R., Usha, R., 2008. Thin Newtonian film flow down a porous inclined plane: stability analysis. Phys. Fluids 20, 022105.

Sadiq, I.M.R., Usha, R., Joo, S.W., 2010. Instabilities in a liquid film flow over an inclined heated porous substrate. Chem. Eng. Sci. 65, 4443–4459.

Sheludko, A., 1967. Thin liquid films. Adv. Colloid Interface Sci. 1, 391–464.

Shkadov, V.Ya., Beloglazkin, A.N., Gerasimov, S.V., 2008. Solitary waves in a viscous liquid film flowing down a thin vertical cylinder. Mosc. Univ. Mech. Bull. 63, 122–128.

Sweetland, M., Lienhard V, J.H., 2000. Evaporative cooling of continuously drawn glass fibers by water sprays. Int. J. Heat Mass Transf. 43, 777–790.

Trevelyan, P.M.J., Kalliadasis, S., 2004a. Dynamics of a reactive falling film at large Péclet numbers. I. Long-wave approximation. Phys. Fluids 16, 3191–3208.

Trevelyan, P.M.J., Kalliadasis, S., 2004b. Dynamics of a reactive falling film at large Péclet numbers. II. Nonlinear waves far from criticality: integral-boundary-layer approximation. Phys. Fluids 16, 3209–3226.

Trevelyan, P.M.J., Kalliadasis, S., Merkin, J.H., Scott, S.K., 2002. Dynamics of a vertically falling film in the presence of a first-order chemical reaction. Phys. Fluids 14, 2402–2421.

Trevelyan, P.M.J., Pereira, A., Kalliadasis, S., 2012. Dynamics of a reactive thin film. Math. Model. Nat. Phenom. 7, 99–145.

Williams, M.B., Davis, S.H., 1982. Nonlinear theory of film rupture. J. Colloid Interface Sci. 90, 220–228.

Witelski, T.P., Bernoff, A.J., 2000. Dynamics of three-dimensional thin film rupture. Phys. D, Nonlinear Phenom. 147, 155–176.

Xie, R., Karim, A., Douglas, J.F., Han, C.C., Weiss, R.A., 1998. Spinodal dewetting of thin polymer films. Phys. Rev. Lett. 81, 1251–1254.

Zeng, Z., Sadeghpour, A., Warrier, G., Ju, Y.S., 2017. Experimental study of heat transfer between thin liquid films flowing down a vertical string in the Rayleigh-Plateau instability regime and a counterflowing gas stream. Int. J. Heat Mass Transf. 108, 830–840.

Zhao, F., Lai, M.C., Harrington, D.L., 1999. Automotive spark-ignited direct-injection gasoline engines. Prog. Energy Combust. Sci. 25, 437–562.